Modeling low-coherence enhanced backscattering using Monte Carlo simulation

Hariharan Subramanian, Prabhakar Pradhan, Young L. Kim, Yang Liu, Xu Li, and Vadim Backman

Constructive interference between coherent waves traveling time-reversed paths in a random medium gives rise to the enhancement of light scattering observed in directions close to backscattering. This phenomenon is known as enhanced backscattering (EBS). According to diffusion theory, the angular width of an EBS cone is proportional to the ratio of the wavelength of light λ to the transport mean-free-path length l_s^* of a random medium. In biological media a large $l_s^* \sim 0.5$–2 mm $\gg \lambda$ results in an extremely small ($\sim$0.001°) angular width of the EBS cone, making the experimental observation of such narrow peaks difficult. Recently, the feasibility of observing EBS under low spatial coherence illumination (spatial coherence length $L_{sc} \ll l_s^*$) was demonstrated. Low spatial coherence behaves as a spatial filter rejecting longer path lengths and thus resulting in an increase of more than 100 times in the angular width of low coherence EBS (LEBS) cones. However, a conventional diffusion approximation-based model of EBS has not been able to explain such a dramatic increase in LEBS width. We present a photon random walk model of LEBS by using Monte Carlo simulation to elucidate the mechanism accounting for the unprecedented broadening of the LEBS peaks. Typically, the exit angles of the scattered photons are not considered in modeling EBS in the diffusion regime. We show that small exit angles are highly sensitive to low-order scattering, which is crucial for accurate modeling of LEBS. Our results show that the predictions of the model are in excellent agreement with the experimental data.

OCIS codes: 030.1670, 290.4210, 290.1350, 290.1990.

1. Introduction

The constructive self-interference effect due to coherent waves traveling in time-reversed paths in a disordered medium produces an enhanced intensity cone in the directions close to the backscattering. In the case of a complete diffusion of light, the amplitude of this intensity profile as a function of the backscattering angle can be as high as twice that of the incoherent background.[1] This increase in reflectivity in the backward direction leads to a reduction in the amount of light transported in the forward direction resulting in the weak localization of the photon. This phenomenon of enhanced backscattering (EBS), also known as coherent backscattering, was first experimentally observed in aqueous suspensions of polystyrene microspheres.[1–3] Thereafter, EBS has become a subject of major research interest.[4–11] To explain the phenomenon of enhanced backscattering, we assume the light to be completely spatially coherent.[4,5] In a homogeneous semi-infinite disordered medium, the full angular width at half-maximum (FWHM), ω_{hm}, of the EBS cone has been shown to be inversely proportional to the ratio of the wavelength of light λ to the transport mean-free-path length l_s^* of light in the medium.[2,3]

$$\omega_{hm} = \lambda/(3\pi\, l_s^*). \tag{1}$$

Although EBS enhancement has been widely studied in a variety of disordered media with relatively short l_s^*,[7–9] the investigation of EBS in weakly scattering media with $l_s^* \gg \lambda$ has been exceedingly difficult, due in part to the very small widths of EBS peaks predicted in such media (e.g., $\omega_{hm} \sim 0.001°$ for $l_s^* \sim 1$ mm) and excessive speckle.[5,10,11] Only recently, in pioneering experiments, Sapienza *et al.*[12] have achieved the detection of such narrow EBS peaks.

The authors are with the Department of Biomedical Engineering, Northwestern University, Evanston, Illinois 60208. H. Subramanian's e-mail address is hariharan@northwestern.edu.

Received 25 August 2005; revised 15 December 2005; accepted 28 March 2006; posted 29 March 2006 (Doc. ID 64419).

0003-6935/06/246292-09$15.00/0

In particular, a biological tissue is one important example of a weakly scattering medium with long l_s*. Measurement of light scattering and the absorption properties of tissue are crucial to exploit the use of light for both diagnostic and therapeutic purposes.[13–20] Accordingly, EBS may be used as one of the potential tools for the noninvasive optical characterization of tissue. However, only very few studies[10,21,22] have actually attempted EBS measurements in tissue. In particular, Yoo *et al.*[21,22] first reported EBS in biological tissue by using femtosecond time-resolved measurements.

Recently, we demonstrated the feasibility of observing EBS under low spatial coherence illumination (spatial coherence length $L_{sc} \ll l_s$*).[23,24] Low spatial coherence behaves as a spatial filter that rejects longer path lengths with exponentially low probability, thus, resulting in an increase of more than 100 times in the angular width of low-coherence EBS (LEBS) cones. Furthermore, we showed that not only does LEBS represent a novel enhanced backscattering phenomenon, but it also opens up the feasibility of studying enhanced backscattering in biological tissue and other media with long l_s* and enables depth-selective spectroscopic tissue characterization.[25] For example, we demonstrated that LEBS can be used to diagnose the earliest, previously undetectable stage of colon carcinogenesis that precedes currently histologically detectable lesions.[23,24] These results underline the need for a thorough understanding of this new effect.

Previously, LEBS was observed by combining EBS measurements with low spatial coherence (LSC) illumination and low temporal coherence detection. This technique uses a broadband continuous wave xenon lamp to achieve low spatial coherence illumination. We also demonstrated that the angular width of an EBS peak observed under LSC illumination ($\sim$0.3°) is more than 100 times broader than that of a conventional EBS.[23] We note that one of the most intriguing properties of LEBS is the dramatically increased angular width of the LEBS peaks, which cannot be explained on the basis of a conventional diffusion approximation based model of EBS alone. To further our understanding of this unprecedented broadening of LEBS peaks and identify the origin of LEBS, it is necessary to develop a rigorous model of LEBS.

In this paper we present the photon random walk model of low-coherence enhanced backscattering by using Monte Carlo (MC) simulations, which is subsequently compared with the experimentally obtained LEBS peaks. MC simulations have been extensively used to simulate light propagation in biological tissue.[26,27] Many groups[28–31] have used the MC modeling of EBS peaks in biological and nonbiological samples. Labeyrie *et al.*[28] reported the first quantitative comparison between the experimentally observed EBS peaks and MC simulation in cold atoms by taking into account the shape of the atomic cloud and its internal structure. Eddowes *et al.*[31] used a MC model of backscattered light from turbid media to simulate weak localization in biological tissues and were able to extract optical parameters such as scattering and absorption coefficients from angular intensity profiles of EBS peaks. Berrocal *et al.*[32] recently characterized intermediate scattering in sprays and other industrially relevant turbid media by using a MC simulation. Specifically, they explained the influence of the exit angle of photons on the relative intensity of different orders of scattering in the intermediate, single-to-multiple scattering regime and validated their results by MC simulation.

In this paper we model LEBS by using MC simulations for what is believed to be the first time. We show that the model is in excellent agreement with experimental data, and we explain the origin of LEBS broadening. We demonstrate that the exit angle of the scattered photons, typically neglected in modeling conventional EBS peaks, is of critical importance when the spatial coherence length of the light source is much smaller than l_s* (i.e., $L_{sc} \ll l_s$*). On the other hand, we show that the exit angle of photons plays only a minimal role in the diffusion regime when the spatial coherence length is greater than l_s* of the medium (i.e., $L_{sc} \gg l_s$*).

The paper is organized as follows: Section 2 describes the theory of LEBS peaks and the MC simulations used in modeling the LEBS profile from a random dielectric medium. Section 3 addresses the importance of the exit angle of photons in low-order scattering regime compared with the diffusive regime. Section 4 explains the validation of our MC model with analytic expression and the comparison with experimental results. Finally, in Section 5 we discuss our results and our conclusions.

2. Monte Carlo Model of Low-Coherence Enhanced Backscattering (LEBS)

To model LEBS, we developed a photon random walk model by using a MC simulation. EBS originates from constructive interference between any given light path and its time-reversed counterpart related by the reciprocity theorem. MC simulation provides a distribution of the photon backscattering intensity as a function of radial distance and exit angle for relevant optical parameters. The shape of the EBS cone versus the scattering angle is calculated from the Fourier transform of the radial intensity distribution on the surface of the sample illuminated by a point source simulated by the MC method. This technique has been successfully used in modeling EBS in nonbiological and biological samples.[30,31,33] The intensity of the EBS cone thus obtained in the backward direction, I_{EBS} can be written as

$$I_{EBS}(\vec{q}_\perp) = \int\int P(r)\exp(iq_\perp.r)\mathrm{d}^2r, \qquad (2)$$

where $P(r)$ is the probability of radial intensity distribution of EBS photons with the radial vector r perpendicular to the incident light and $q_\perp$ is the projection of the wave vector onto the orthogonal plane in

the backward direction. In an isotropic disordered medium, the two-dimensional Fourier integral can be further simplified to[24]

$$I_{\mathrm{EBS}}(\vec{q}_{\perp}) \propto \int rP(r)\exp(iq_{\perp}.r)\mathrm{d}r, \quad (3)$$

where $rP(r)$ is the radial intensity distribution of the conjugated time-reversed paths around a pointlike light source illuminating a sample and the projection of wave vector $q_{\perp} = 2\pi \sin\theta/\lambda$.

In contrast to conventional EBS, LEBS is observed by using a broadband light source with low spatial coherence.[23] Therefore to model the effect of a low spatial coherence length of illumination on EBS, we incorporated an additional coherence length dependent weighting factor to the numerical simulation. We used the readily derived form of the degree of spatial coherence $C_{L_{\mathrm{sc}}}(r)$ as follows[34]:

$$C_{L_{\mathrm{sc}}}(r) = 2J_1(r/L_{\mathrm{sc}})/(r/L_{\mathrm{sc}}), \quad (4)$$

where J_1 is the first-order Bessel function, L_{sc} is the spatial coherence length corresponding to the 88th percentile of the ideal value of unity, and r is the radial vector perpendicular to the incident light. Thus the modified LEBS intensity in the presence of a low coherence source can be written as

$$I_{\mathrm{LEBS}}(\theta) \propto \int rP(r).C_{L_{\mathrm{sc}}}(r)\exp\left(i\,\frac{2\pi \sin\theta}{\lambda}\,r\right)\mathrm{d}r. \quad (5)$$

The first term in Eq. (5), $rP(r)$ [$\equiv I(r)$], is the radial intensity distribution of the pointlike source illuminating the sample, which can be obtained using the MC simulation.

A detailed description of the MC simulation is given in Refs. 35 and 36. Here we only briefly describe the essential aspects of this method. In our simulations, approximately 10^{10} photon packets were launched into the sample. The optical parameters of the sample were assigned based on the sample size used in the LEBS experiment.[23] The samples were slabs with infinite lateral extents (sample thickness = 50 mm) and had optical parameters of biological relevance (l_s^* 500–2000 μm, $g \sim 0.6$–0.9, $\lambda = 520$ nm). The direction of incidence was normal to the sample's surface (the xy plane) with an initial weight w. As the specular reflectance was completely avoided in the experiment, the photon packets were allowed to propagate within the sample with its initial weight of w and random step size s, given as $s = -\ln(\xi)/\mu_t$, where μ_t is the total interaction coefficient of the medium, and ξ is the pseudorandom number uniformly distributed between 0 and 1. Once the photon packet reached the interaction site, a scattering direction was then defined by the deflection angle θ ($0 < \theta < \pi$) and azimuthal angle φ ($0 < \varphi < 2\pi$), which were statistically sampled. The probability distribution of the cosine of the deflection angle was chosen according to the Henyey–Greenstein anisotropic phase scattering probability function[37] given as

$$P_{\mathrm{HG}}(\cos\theta) = (1-g^2)/\left[2(1+g^2-2g\cos\theta)^{3/2}\right], \quad (6)$$

where $\langle\cos(\theta)\rangle = g$. We assumed the angular distribution to be azimuthally symmetrical, i.e., a uniform distribution for $\varphi(=2\pi\xi)$, such that $P_{\varphi}(\varphi) = 1/(2\pi)$. The photon packet was terminated by using the Russian roulette technique[38] after it underwent a series of scattering events. The weight of the photon packets escaping from the medium in the forward or backward direction, was then recorded in a user defined grid system.

Our study is focused on the intensity profile of photons in the backward direction from low-order scatterings. The radial and angular resolution of the grid system used in the MC simulation to collect the low-order scattering photons was specified as 1 μm and 0.3°, respectively. The optical parameters, such as the scattering coefficients and transport mean free path of the scattering medium, were obtained from the sample used in the experiment.

Once the reflectance probability $P(r)$ was calculated from the MC simulation, Eq. (5) was then used to obtain the LEBS peak by using the Fourier transform of the radial intensity distribution. The LEBS peak obtained was then convoluted with the angular response of the instrument (~0.04°–0.3°) to compensate for the finite point-spread function of the detection system and the slight divergence of the incident beam. The width of the convoluted LEBS peak W is defined as follows[39]:

$$W = \left(\int_0^{\infty} I_{\mathrm{LEBS}}(\vec{q}_{\perp})\mathrm{d}\vec{q}_{\perp}\right)^2 \Big/ \left[\int I_{\mathrm{LEBS}}{}^2(\vec{q}_{\perp})\mathrm{d}\vec{q}_{\perp}\right]. \quad (7)$$

According to our simulations W provides a better metric to characterize LEBS peak width compared to FWHM. The width obtained from the simulation was then compared with those obtained from the LEBS experiment.

3. Results

A. Effect of Exit Angle of Photons in Low Orders of Scattering

We first obtained the radial intensity distributed on the surface of the sample with $l_s^* = 2$ mm. The absorption coefficient μ_a and scattering coefficient μ_s were fixed at 0.0001 and 5 mm^{-1} (at $\lambda = 520$ nm), respectively. The radial intensity distribution was calculated from the MC simulation at different exit angles between 0.3° and 90°. The normalized intensity in arbitrary units (A.U.) at three different exit angles (1.5°, 20°, and 80°) is shown in Fig. 1. The radial and angular resolution of the grid system used in the MC simulation to collect the diffusive multiple

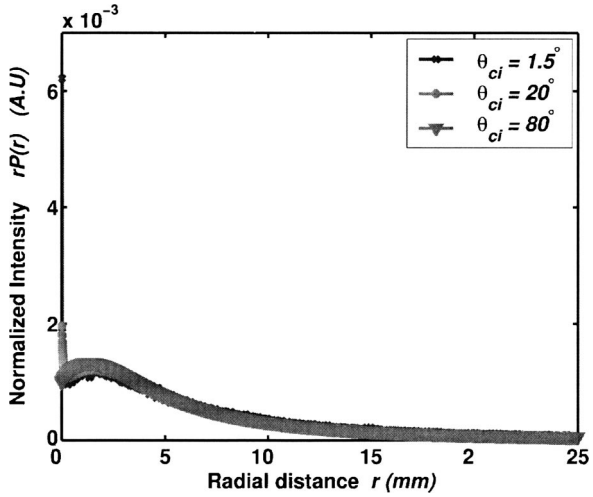

Fig. 1. Normalized intensity at different exit angles, θ_{ci} in the diffusive multiple scattering regime ($L_{sc} \gg l_s^*$) is plotted as a function of radial distance r. Intensities are calculated by using MC simulation from a medium with $l_s^* = 2$ mm, $g = 0.9$ (at $\lambda = 520$ nm) and $L_{sc} = 50$ mm. Intensity profiles for different exit angles remain constant in the diffusive multiple scattering regime.

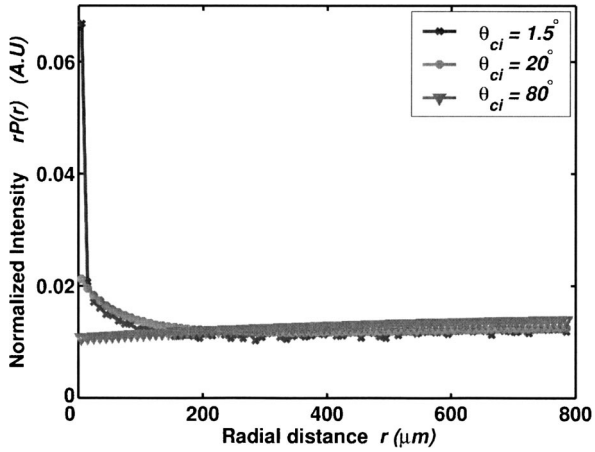

Fig. 2. Normalized intensity at different exit angles, θ_{ci} in the low-order scattering regime ($L_{sc} \ll l_s^*$) is plotted as a function of radial distance r. Intensities are calculated using by MC simulation ($l_s^* = 2$ mm, $g = 0.9$ at $\lambda = 520$ nm) with $L_{sc} = 600$ μm. When the number of scattering events is restricted due to the finite spatial coherence area by using a low spatial coherence illumination, the intensity profile over r becomes broader as θ_{ci} increases from 1.5° to 80°.

scattering photons is specified as 10 μm and 0.3°, respectively. Typically in the diffusion regime, the EBS peak is obtained directly from the Fourier transform of the radial intensity without taking into account the exit angle of the photons. From Fig. 1 it can be seen that the intensity profile for diffusive multiple scattering remains constant for different exit angles. This intensity profile obtained above can be written as

$$\int_{r=0}^{\infty}\int_{\theta=0}^{\pi/2} p(r,\ \theta)\mathrm{d}r\mathrm{d}\theta = N, \tag{8}$$

(for $\mu_a = 0$ and transmission = 0), where N is the total number of photons injected. Let us now redefine the above probability integral for any finite angle as follows:

$$\int_{r=0}^{\infty}\int_{\theta=0}^{\theta ci} p(r,\ \theta)\mathrm{d}r\mathrm{d}\theta = \int_{r=0}^{\infty} \bar{p}_{\theta_{ci}}(r)\mathrm{d}r = N_{\infty,ci}. \tag{9}$$

Now we normalize the above probability along the radial direction keeping the maximum angles θ_{ci} ($i = 1, 2, 3, \ldots$) fixed.

Let, $\bar{p}_{\theta_{ci}}(r)/N_{\infty,ci} = P_{\theta_{ci}}(r)$; thus

$$\int_{0}^{\infty} P_{\theta_{ci}}(r)\mathrm{d}r = 1. \tag{10}$$

We now consider three different angles, $\theta_{c1} = 1.5°$, $\theta_{c2} = 20°$, and $\theta_{c3} = 80°$. The shape of the $P_{\theta_{ci}}(r)$, ($i = 1, 2,$ and 3) curves remains constant, which is shown in Fig. 1. However, a different picture emerges in the case of low spatial coherence illumination when the number of scattering events is restricted by using a low spatial coherence light source. $P_{\theta_{ci}}(r)$ becomes broader as θ_{ci} increases from 1.5° to 80°, as shown in Fig. 2.

In case of the spatial coherence light source the above probability distribution can be written as

$$\int_{r=0}^{Lsc}\int_{\theta=0}^{\pi/2} p(r,\ \theta)\mathrm{d}r\mathrm{d}\theta = N_{Lsc}, \tag{11}$$

where N_{Lsc} is the number of photons restricted by finite spatial area using low spatial coherence illumination, and,

$$\int_{0}^{Lsc}\int_{0}^{\theta ci} p(r,\ \theta)\mathrm{d}r\mathrm{d}\theta = \int_{0}^{Lsc} \bar{p}_{\theta_{ci}}(r)\mathrm{d}r = N_{Lsc,ci}. \tag{12}$$

Let $\bar{p}_{\theta_{ci}}(r)\mathrm{d}r/N_{Lsc,ci} = P_{\theta_{ci}}(r)$; thus

$$\int_{0}^{Lsc} P_{\theta_{ci}}(r)\mathrm{d}r = 1. \tag{13}$$

We point out that contrary to the diffusion regime, the shapes of $P_{\theta_{ci}}(r)$ in the low-order scattering regime are different. The shape of $P_{\theta_{c1}}(r)$ is much narrower than that of $P_{\theta_{c2}}(r)$. For small radial distances corresponding to only few scattering events, it can be shown that

$$\int_{0}^{Lsc/10} P_{\theta_{c1}}(r)\mathrm{d}r \gg \int_{0}^{Lsc/10} P_{\theta_{c2}}(r)\mathrm{d}r. \tag{14}$$

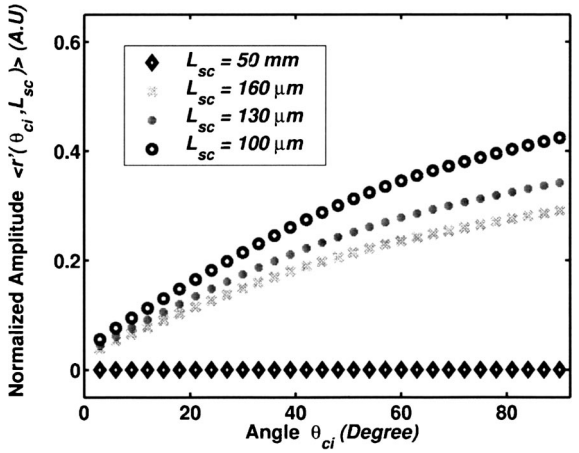

Fig. 3. $\langle r'(\theta_{ci}, L_{sc})\rangle$ as a function of exit angle θ_{ci} for four different L_{sc}. $\langle r'(\theta_{ci}, L_{sc})\rangle$ is simulated for a sample with $l_s^* = 2$ mm and $g = 0.9$ (at $\lambda = 520$ nm) for different exit angles θ_{ci} varying from 1° to 90°. $\langle r'(\theta_{ci}, L_{sc})\rangle$ is insensitive to the exit angle θ_{ci} when $L_{sc} \gg l_s^*$, while $\langle r'(\theta_{ci}, L_{sc})\rangle$ increases with the increase in the exit angle in the low order scattering regime ($L_{sc} \ll l_s^*$).

This result indicates the importance of considering the exit angles of photons particularly for modeling low coherence enhanced backscattering peaks.

As discussed before, the exit angles are less sensitive in the multiple scattering regime providing similar EBS peaks for different exit angles. In the diffusion regime, the slight changes in reflectance probability $P(r)$ obtained from MC simulation at different exit angles are translated over a radial distance of approximately 50 mm. Hence these small changes do not translate into a narrow–broad peak when the Fourier transform of $P(r)$ is performed. To explain this fact we consider a function

$$\langle r'(\theta_{ci},\ L_{sc})\rangle = \int_0^{Lsc} \frac{rP_{\theta_{c1}}(r)\mathrm{d}r}{L_{sc}}. \tag{15}$$

As expected, Fig. 3 shows that $\langle r'(\theta_{ci}, L_{sc})\rangle$ remains constant with the change in exit angle in the EBS regime ($L_{sc} = 50$ mm $\gg l_s^*$). On the other hand, in the low-coherence regime ($L_{sc} = 200$ μm $\ll l_s^*$), we expect to see a change in the above function $\langle r'(\theta_{ci}, L_{sc})\rangle$ since the changes in $P(r)$ for different angles of collection are only translated over a very small radial distance. This effect is illustrated in Fig. 3, which shows that in a low-coherence regime, $\langle r'(\theta_{ci}, L_{sc})\rangle$ increases with the increase in exit angle. It is also shown that the slope of the curve increases as the spatial coherence length L_{sc} decreases from 160 to 100 μm. Hence in a low-coherence regime, obtaining $P(r)$ for different angles of collection significantly affects the width of the LEBS peaks. Therefore it is imperative to obtain a proper exit angle to accurately model the LEBS peak in the low-order scattering regime. This aspect is further explored in the subsequent subsections.

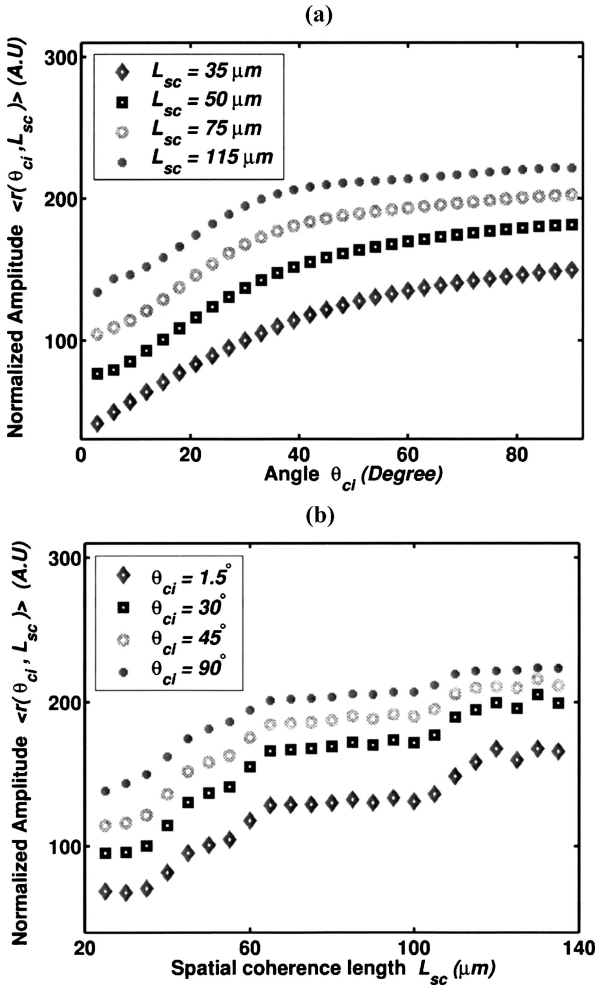

Fig. 4. (a) $\langle r(\theta_{ci}, L_{sc})\rangle$ as a function of angle θ_{ci} obtained for four different L_{sc}. (b) $\langle r(\theta_{ci}, L_{sc})\rangle$ as a function of L_{sc} obtained for four different θ_{ci}. $\langle r(\theta_{ci}, L_{sc})\rangle$ is calculated by using MC simulation from a medium with $l_s^* = 2$ mm and $g = 0.9$ (at $\lambda = 520$ nm for θ_{ci} varying from 1° to 90° and different L_{sc} varying between 35 and 140 μm. $\langle r(\theta_{ci}, L_{sc})\rangle$ is proportional to both θ_{ci} and L_{sc}.

B. Importance of Proper Exit Angle in Accurate Modeling of Low-Coherence Enhanced Backscattering Peaks

Subsection 3.A clarified that the exit angle of photons in the image plane is of critical importance for low-coherence enhanced backscattering as LEBS probes low orders of scattering in a diffusive multiple scattering medium. This is because the trajectories of the photons are clustered into a compact locus to exit at small angles for low orders of scattering, while the trajectories of the photons are less compact for higher orders of scattering. As can be seen from our simulations, the exit angle of the photons is sensitive to the depth from which the LEBS measurements are obtained. This fact is further illustrated in Figs. 4(a) and 4(b), which show $\langle r(\theta_{ci}, L_{sc})\rangle$ calculated for different exit angles and different spatial coherence length L_{sc}.

$$\langle r(\theta_{ci},\ L_{sc})\rangle = \int_0^{Lscj} rP_{\theta_{ci}}(r)\mathrm{d}r, \tag{16}$$

where $i = 0°$ to 90° and $j = 20$ to 140 μm.

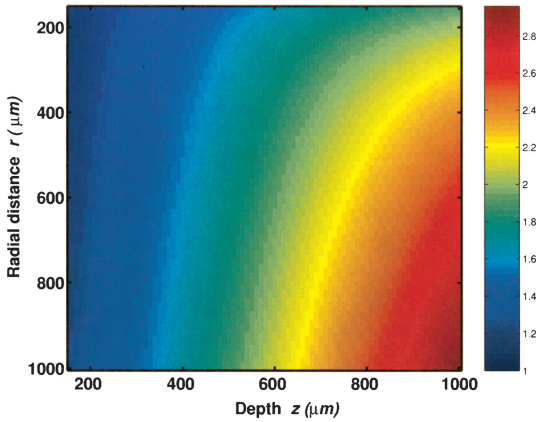

Fig. 5. $\langle r(\theta_{ci}, L_{sc})\rangle$ as a function of r and depth of penetration of scattered photons z for a fixed $\theta_{ci} = 45°$ and a fixed $L_{sc} = 600$ μm. $\langle r(\theta_{ci}, L_{sc})\rangle$ is calculated from a medium with $l_s^* = 2$ mm and $g = 0.9$ (at $\lambda = 520$ nm) by using MC simulation. $\langle r(\theta_{ci}, L_{sc})\rangle$ is proportional to the penetration depth z.

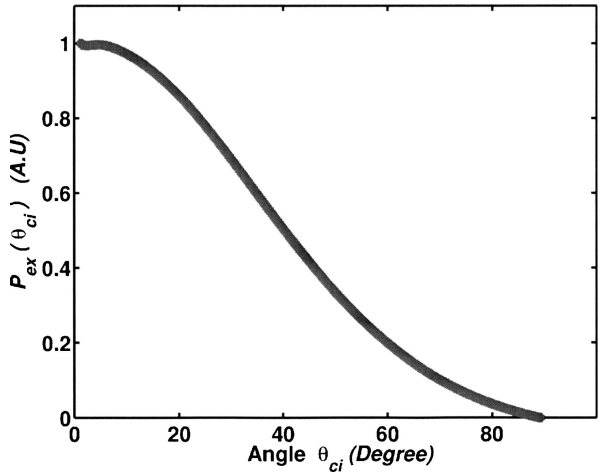

Fig. 6. Probability of exit angle $P_{ex}(\theta_{ci})$ as a function of θ_{ci} obtained for low-order scattering regime. $P_{ex}(\theta_{ci})$ is calculated by using MC simulation ($l_s^* = 2$ mm, $g = 0.9$ at $\lambda = 520$ nm) for a fixed $L_{sc} = 200$ μm by varying θ_{ci} between 1° and 90°. $P_{ex}(\theta_{ci})$ converges at small angles of approximately 1°–3° when $L_{sc} \ll l_s^*$.

As shown in Fig. 4(a), for a given L_{sc}, $\langle r(\theta_{ci}, L_{sc})\rangle$ increases with the increase of the exit angle from 0° to 90°. Similarly, for a fixed exit angle, an increase in L_{sc} from 20 to 140 μm leads to an increase in $\langle r(\theta_{ci}, L_{sc})\rangle$ as also shown in Fig. 4(b). The relationship between $\langle r(\theta_{ci}, L_{sc})\rangle$ and the depth of penetration of the scattered photons are obtained by using MC simulation by tracking the propagation of photons along the z direction. The simulation is performed in the low-order scattering regime and the size of the grid tracking the photons in the z direction is kept at 1 μm. Figure 5 shows this relationship that indicates that $\langle r(\theta_{ci}, L_{sc})\rangle$ is proportional to the depth from which the photons are scattered in the backward direction.

To model LEBS, it is necessary to accurately determine the angle at which the photons are collected. The LEBS signals obtained from the simulation are collected at $\theta_{ci} \sim 1.5°$, which is close to the width of the experimentally recorded LEBS peaks. This is because the angular range of the photons traveling in the time-reversed direction restricts the exit angle of the photons in the LEBS experiments. It can be seen from Fig. 6 that the probability of exit angle, $P_{ex}(\theta_{ci})$ remains almost identical at small angles at approximately 0.3°–3° when spatial coherence light source is used. Therefore we take the midpoint of this distribution (~1.5°) at small angles for a better averaging of $P(r)$. The LEBS peak width obtained from exit angles, $\theta_{ci} \sim 1.5°$ deviates less than 5% when compared to the photons collected at low exit angles (0.3° to 1°). However, any change in the exit angle of the photons beyond this would significantly change the depth from which the time-reversed photons are obtained leading to erroneous modeling of LEBS. We obtain $P(r)$ at 1.5° by using MC simulation and then multiply it by the spatial coherence function [Eq. (4)] corresponding to the coherence length used in the experiment. The Fourier transform of this multiplied product is then taken to obtain the LEBS peak. In Subsections 3.C and 3.D we present detailed validation of the LEBS peak obtained by using MC simulation by comparing with analytical model and LEBS experiments.

C. Validation of Low-Coherence Enhanced Backscattering Monte Carlo Simulations

To verify the accuracy of the MC simulation, we first compare the profile of the EBS peak obtained from numerical simulation with the profile of the EBS peak calculated by Akkermans *et al.*[40] for an isotropic scattering medium. The simulation is performed

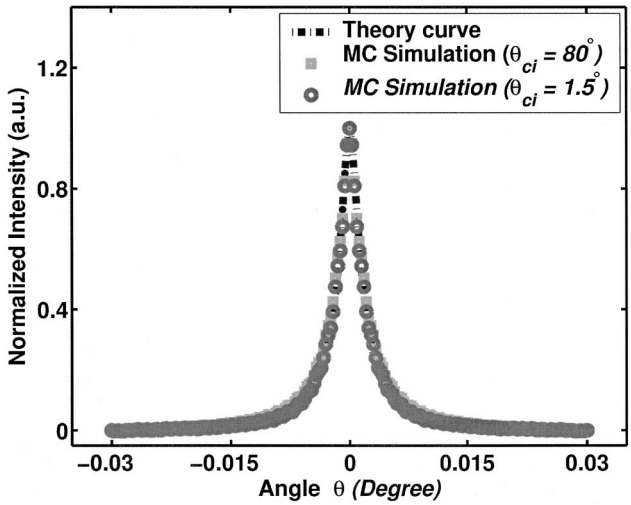

Fig. 7. Comparison of the EBS profile from MC simulation with that from analytical formulation (Ref. 40). Profile of the EBS peak from MC simulation $I_{EBS}(\theta)$, is calculated from a medium with $l_s^* = 2$ mm and $g = 0.9$ (at $\lambda = 520$ nm) for $L_{sc} = 50$ mm. Results from the simulation are in excellent agreement with the analytical results. Also, the LEBS simulation for $\theta_{ci} = 1.5°$ agrees well with the results obtained from $\theta_{ci} = 80°$ as the width of the EBS peak is insensitive to the θ_{ci} in the diffusive multiple scattering regime ($L_{sc} \gg l_s^*$).

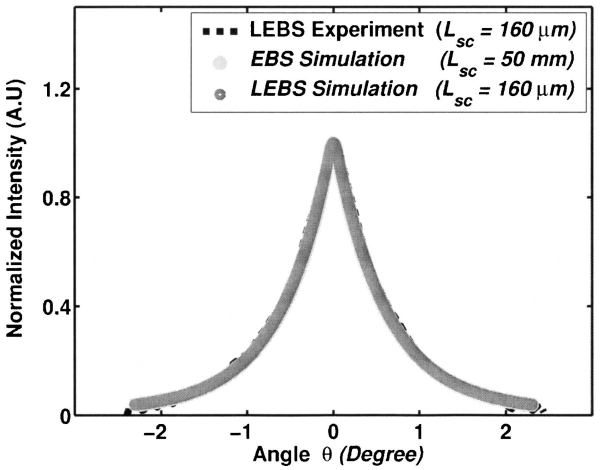

Fig. 8. Normalized intensity profile of the LEBS peak as a function of θ from MC simulation is compared with that of the experimental result from white paint under low spatial coherence illumination (Xenon lamp, λ = 520 nm, L_{sc} = 160 μm). $L_{LEBS}(\theta)$, is calculated by using MC simulation from a medium with l_s^* = 4 mm and g = 0.9 (at λ = 520 nm) for L_{sc} = 160 μm. Simulation results agree well with experimentally observed LEBS peak when L_{sc} = 160 μm. Also, the EBS peak from L_{sc} = 50 mm and LEBS peak from L_{sc} = 160 μm are completely indistinguishable as the peak width is completely determined by the small l_s^* of the medium and the spatial coherence length plays an insignificant role in this regime.

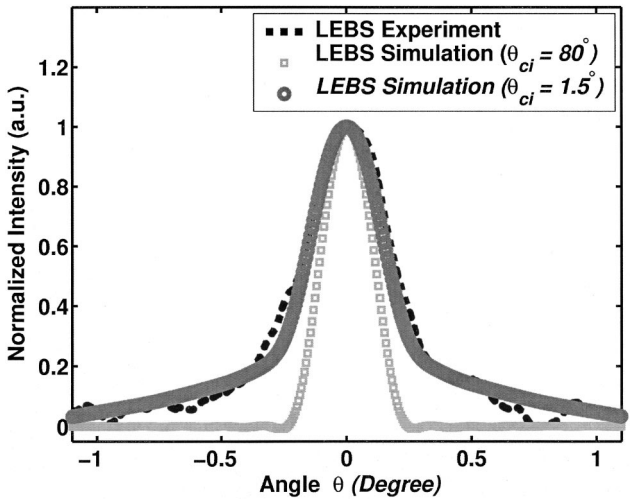

Fig. 9. Normalized intensity profile of the LEBS peak as a function of angle θ from MC simulation is compared with that of the aqueous suspensions of polystyrene microspheres (diameter = 0.89 μm) under low spatial coherence illumination (Xenon lamp, λ = 520 nm, L_{sc} = 48 μm). $L_{LEBS}(\theta)$, is simulated for a medium with l_s^* = 2 mm, g = 0.9 (at λ = 520 nm), and L_{sc} = 48 μm. LEBS peak simulated by MC simulation at θ_{ci} = 1.5° matches well with the LEBS peak profile recorded in the experiment. On the contrary, the LEBS peaks from θ_{ci} = 80° are three times narrower than those obtained from the experiment and the large angles do not accurately predict the LEBS peak as they are insensitive to low orders of scattering.

with l_s^* = 2 mm and infinite spatial coherence (L_{sc} = 50 mm), with the exit angle, $\theta_{ci} \approx 1.5°$. Figure 7 shows that the simulation results match well with the analytical results. To verify the effect of exit angles in EBS measurements, the simulations from small exit angles, $\theta_{ci} \approx 1.5°$, are compared to those obtained from higher exit angles (e.g., θ_{ci} = 80°). As shown in Fig. 7, the MC simulation for smaller exit angle (circles) agrees with the results obtained from large exit angles (squares).

We next validate the spatial coherence function [Eq. (4)] used in simulating the LEBS peak by comparing the profiles obtained from the simulation with those of the LEBS experiments (discussed in Subsection 3.D) for a sample with l_s^* smaller than L_{sc}. In this regime ($l_s^* \ll L_{sc}$), though L_{sc} is small, LEBS profiles are primarily determined by l_s^* as the light scattering paths are not affected by the L_{sc} and hence the role of the finite L_{sc} is virtually insignificant. We simulate the LEBS peak with L_{sc} = 160 μm from a sample of l_s^* = 4 μm. The LEBS peak in the experiment is collected from white paint (Benjamin Moore) with l_s^* = 4 μm under low spatial coherence illumination (Xenon lamp). As shown in Fig. 8, the LEBS peak obtained from MC simulation matches well with the experimentally observed LEBS peak for $l_s^* \ll L_{sc}$. This validates the use of spatial coherence function in the modeling of LEBS peak for low spatial coherence illumination. We further compare the LEBS profile with the EBS peak obtained from infinite spatial coherence length (L_{sc} = 50 mm). As expected, the EBS and LEBS peaks are completely indistinguishable as the peak width is completely determined by the small l_s^* of the medium (see Fig. 8). In the Subsection 3.D we present the experimental verification of the LEBS simulation in the low-order scattering regime ($L_{sc} \ll l_s^*$).

D. Comparison of Monte Carlo Simulation with the Experimental Results

The LEBS peak obtained by using MC simulations was experimentally verified. The detailed description of our experimental setup is given elsewhere.[23,24] Here we describe the essential parts in brief. The experimental setup consisted of a 500 W Xe lamp (Oriel) to deliver a CW broadband light that was then collimated by using a 4-f lens system. The collimated light was polarized and delivered onto a sample at an incident angle of 15° to prevent specular reflection. The spatial coherence length of illumination L_{sc} varied between 30 and 220 μm, which was confirmed by a double-slit interference experiment.[34] The backscattered light from the sample was sent through a setup consisting of a Fourier lens and a polarizer oriented along the same direction of the incident light. The copolarized light was then collected by an imaging spectrograph (Acton Research) positioned in the focal plane of the Fourier lens and coupled to a CCD camera (CoolsnapHQ, Roper Scientific). The angular distribution of the backscattered light from the sample was projected onto the slit of the spectrograph, which dispersed the light according to the wavelength in the direction perpendicular to the slit. The CCD camera recorded a matrix of light scattering

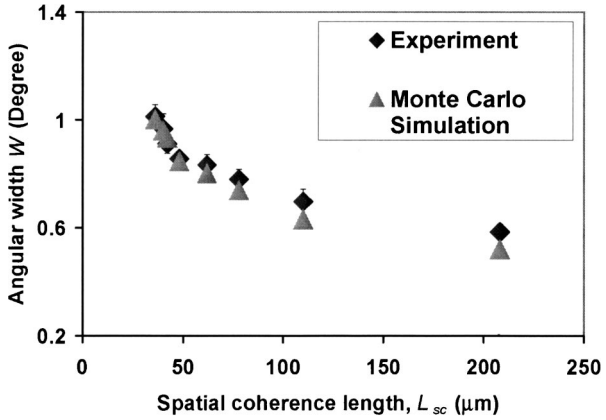

Fig. 10. Comparison of angular width W of the LEBS peaks obtained from MC simulation with that of LEBS peaks from experiment (bead diameter = 0.89 μm) under low spatial coherence illumination (Xenon lamp, $\lambda = 520$ nm). The width of LEBS peak from simulation ($l_s^* = 2$ mm, $g = 0.9$ at $\lambda = 520$ nm) is calculated for eight different L_{sc} varying between 30 and 220 μm at a fixed $\theta_{ci} = 1.5°$. The error bars in the curves are the standard errors. The widths of the LEBS peaks predicted by MC simulation are in excellent agreement with those determined from the experiment.

intensity as a function of backscattering angle θ at different wavelengths λ. In each CCD pixel, the collected light was integrated within a narrow band of wavelengths around λ, with the width of the band determined by the width of the spectrograph slit. The LEBS peaks were normalized by the incoherent baseline measured at large backscattering angles ($\theta > 4°$). The resulting LEBS signal was compared with the signals predicted by MC simulation.

We recorded LEBS from aqueous suspensions of polystyrene microspheres (Duke Scientific, Palo Alto, California) of various diameters from 200 to 890 nm. The dimension of the samples was $\pi \times 50^2$ mm^2 $\times$ 100 mm. We varied the transport mean-free-path l_s^* from 500 to 2000 μm and the spatial coherence lengths from 30 to 220 μm. As a representation, we show here the results obtained from the sample of $l_s^* = 2000$ μm with a bead diameter of 0.89 μm. As shown in Fig. 9, the LEBS peak predicted by MC simulations is in excellent agreement with the peak recorded in the experiment ($L_{sc} = 48$ μm). Further, the LEBS peak obtained from the higher exit angles (squares) does not accurately model the LEBS peak as it is insensitive to the low orders of scattering. On the other hand, the broadening of LEBS peak can be accurately obtained only at low exit angles (circle) as it is more sensitive to the low orders of scattering. The simulations are further verified for eight other values of L_{sc} varying from 35 to 220 μm (Fig. 10). The error bars in the curves are the standard errors obtained from three different sets of experiments conducted at different spatial coherence lengths. As shown in Fig. 10, the widths of the LEBS peaks predicted by the MC simulations are in excellent agreement with those determined in the experiment. This confirms that the MC simulation can be used to model LEBS.

4. Conclusion

We have demonstrated what we believe to be the first time that the photon random walk model has been used to model low-coherence enhanced backscattering from a weakly scattering medium. We have shown that the LEBS predicted by the simulations are in excellent agreement with the experimental data. Furthermore, we have demonstrated that the exit angles of the photons, which are typically neglected in the modeling of conventional EBS, play a key role in the modeling of LEBS. Since EBS peaks depend on the Fourier transform of the radial distribution of the intensity on the surface of the sample, it is extremely important to consider the change due to the exit angle of the photons in the shape of probability distribution $P(r)$. Our data indicate that the $P(r)$ obtained from low-order scattering is sensitive to the exit angles of the photons, which in turn depend on the depth from which the photons are collected.

This study was supported in part by the National Institutes of Health grants R01 EB003682, R01 CA112315, R01 CA097966, and R21 CA122017, the National Science Foundation grant BES-0238903, and a grant from the Wallace H. Coulter Foundation.

References

1. Y. Kuga and A. Ishimaru, "Retroreflectance from a dense distribution of spherical particles," J. Opt. Soc. Am. A **1,** 831–835 (1984).
2. M. B. van der Mark, M. P. van Albada, and A. Lagendijk, "Light scattering in strongly scattering media: multiple scattering and weak localization," Phys. Rev. B **37,** 3575–3592 (1988).
3. P. E. Wolf, G. Maret, E. Akkermans, and R. Maynard, "Optical coherent backscattering by random media: an experimental study," J. Phys. (Paris) **49,** 63–75 (1988).
4. R. Lenke and G. Maret, "Magnetic field effects on coherent backscattering of light," Eur. Phys. J. B **17,** 171–185 (2000).
5. M. Tomita and H. Ikari, "Influence of finite coherence length of incoming light on enhanced backscattering," Phys. Rev. B **43,** 3716–3719 (1991).
6. A. Wax, S. Bali, and J. E. Thomas, "Time-resolved phase-space distributions for light backscattered from a disordered medium," Phys. Rev. Lett. **85,** 66–69 (2000).
7. A. Dogariu, J. Uozumi, and T. Asakura, "Enhancement of the backscattered intensity from fractal aggregates," Waves Random Media **2,** 259–263 (1992).
8. G. Labeyrie, F. de Tomasi, J. C. Bernard, C. A. Muller, C. Miniatura, and R. Kaiser, "Coherent backscattering of light by cold atoms," Phys. Rev. Lett. **83,** 5266–5269 (1999).
9. D. S. Wiersma, M. P. van Albada, and A. Lagendijk, "Coherent backscattering of light from amplifying random media," Phys. Rev. Lett. **75,** 1739–1742 (1995).
10. G. Yoon, D. N. G. Roy, and R. C. Straight, "Coherent backscattering in biological media: measurement and estimation of optical properties," Appl. Opt. **32,** 580–585 (1993).
11. S. Eternad, R. Thompson, and M. J. Andrejco, "Weak localization of photons: termination of coherent random walks by absorption and confined geometry," Phys. Rev. Lett. **59,** 1420–1423 (1987).
12. R. Sapienza, S. Mujumdar, C. Cheung, A. G. Yodh, and D.

Wiersma, "Anisotropic weak localization of light," Phys. Rev. Lett. **92,** 033903 (2004).
13. Y. L. Kim, Y. Liu, R. K. Wali, H. K. Roy, M. J. Goldberg, A. K. Kromin, K. Chen, and V. Backman, "Simultaneous measurement of angular and spectral properties of light scattering for characterization of tissue microarchitecture and its alteration in early precancer," IEEE J. Sel. Top. Quantum Electron. **9,** 243–256 (2003).
14. K. Sokolov, R. A. Drezek, K. Gossage, and R. R. Richards-Kortum, "Reflectance spectroscopy with polarized light: is it sensitive to cellular and nuclear morphology?" Opt. Express **5,** 302–317 (1999).
15. A. Wax, C. H. Yang, V. Backman, K. Badizadegan, C. W. Boone, R. R. Dasari, and M. S. Feld, "Cellular organization and substructure measured using angle-resolved low-coherence interferometry," Biophys. J. **82,** 2256–2264 (2002).
16. J. R. Mourant, I. J. Bigio, J. Boyer, R. L. Conn, T. Johnson, and T. Shimada, "Spectroscopic diagnosis of bladder cancer with elastic light scattering," Lasers Surg. Med. **17,** 350–357 (1995).
17. V. Backman, M. B. Wallace, L. T. Perelman, J. T. Arendt, R. Gurjar, M. G. Muller, Q. Zhang, G. Zonios, E. Kline, T. McGillican, S. Shapzhay, T. Valdez, K. Badizadegan, J. M. Crawford, M. Fitzmaurice, S. Kabani, H. S. Levin, M. Seiler, R. R. Dasari, I. Itzkan, J. Van Dam, and M. S. Feld, "Detection of preinvasive cancer cells," Nature **406,** 35–36 (2000).
18. S. L. Jacques, J. C. Ramella-Roman, and K. Lee, "Imaging skin pathology with polarized light," J. Biomed. Opt. **7,** 329–340 (2002).
19. L. T. Perelman, V. Backman, M. Wallace, G. Zonios, R. Manoharan, A. Nusrat, S. Shields, M. Seiler, C. Lima, T. Hamano, I. Itzkan, J. Van Dam, J. M. Crawford, and M. S. Feld, "Observation of periodic fine structure in reflectance from biological tissue: a new technique for measuring nuclear size distribution," Phys. Rev. Lett. **80,** 627– 630 (1998).
20. Q. Liu and N. Ramanujam, "Experimental proof of the feasibility of using angled fiber-optic probe for depth-sensitive fluorescence spectroscopy of turbid media," Opt. Lett. **29,** 2034–2036 (2004).
21. K. M. Yoo, G. C. Tang, and R. R. Alfano, "Coherent backscattering of light from biological tissues," Appl. Opt. **29,** 3237–3239 (1990).
22. K. M. Yoo, F. Liu, and R. R. Alfano, "Biological materials probed by the temporal and angular profiles of the backscattered ultrafast laser pulses," J. Opt. Soc. Am. B **7,** 1685–1693 (1990).
23. Y. L. Kim, Y. Liu, V. M. Turzhitsky, H. K. Roy, R. K. Wali, and V. Backman, "Coherent backscattering spectroscopy," Opt. Lett. **29,** 1906–1908 (2004).
24. Y. L. Kim, Y. Liu, R. K. Wali, H. K. Roy, and V. Backman, "Low-coherent backscattering spectroscopy for tissue characterization," Appl. Opt. **44,** 366–377 (2005).
25. Y. L. Kim, Y. Liu, V. M. Turzhitsky, R. Wali, H. Roy, and V. Backman, "Depth-resolved low-coherent backscattering in tissue," Opt. Lett. **30,** 741–743 (2005).
26. B. C. Wilson and G. Adam, "A Monte Carlo model for the absorption and flux distributions of light in tissue," Med. Phys. **10,** 824–830 (1983).
27. L. H. Wang, W. R. Chen, and R. E. Nordquist, "Optimal beam size for light delivery to absorption-enhanced tumors buried in biological tissues and effect of multiple beam delivery: a Monte Carlo study," Appl. Opt. **36,** 8286–8291 (1997).
28. G. Labeyrie, D. Delande, C. A. Muller, C. Miniatura, and R. Kaiser, "Coherent backscattering of light by an inhomogeneous cloud of cold atoms," Phys. Rev. A **67,** 033814 (2003).
29. V. L. Kuzmin and I. V. Meglinski, "Coherent multiple scattering effects and Monte Carlo method," JETP Lett. **79,** 109–112 (2004).
30. R. Lenke, R. Tweer, and G. Maret, "Coherent backscattering of turbid samples containing large Mie spheres," J. Opt. A, Pure Appl. Opt. **4,** 293–298 (2002).
31. M. H. Eddowes, T. N. Mills, and D. T. Delpy, "Monte-Carlo simulations of coherent backscatter for identification of the optical coefficients of biological tissue *in vivo*," Appl. Opt. **34,** 2261–2267 (1995).
32. E. Berrocal, D. Y. Churmakov, V. P. Romanov, M. C. Jermy, and I. V. Meglinski, "Crossed source-detector geometry for a novel spary diagnostic: Monte Carlo simulation and analytical results," Appl. Opt. **44,** 2519–2529 (2005).
33. R. Lenke and G. Maret, *Multiple Scattering of Light: Coherent Backscattering and Transmission, Scattering in Polymeric and Colloidal Systems,* W. Brown and K. Mortensen, eds. (London, Gordon and Breach, 2000), pp. 1–73.
34. M. Born and E. Wolf, *Principles of Optics: Electromagnetic Theory of Propagation, Interference and Diffraction of Light,* 7th ed. (Cambridge U. Press, 1999), pp. 572–580.
35. L. H. Wang, S. L. Jacques, and L. Q. Zheng, "MCML—Monte Carlo modeling of photon transport in multi-layered tissues," Comput. Methods Programs Biomed. **47,** 131–146 (1995).
36. S. P. Lin, L. H. Wang, S. L. Jacques, and F. K. Tittel, "Measurement of tissue optical properties using oblique incidence optical fiber reflectometry," Appl. Opt. **36,** 136–143 (1997).
37. L. G. Henyey and J. L. Greenstein, "Diffuse radiation in the galaxy," Astrophys. J. **93,** 70–83 (1941).
38. J. S. Hendricks and T. E. Booth, "MCNP variance reduction overview," Lect. Notes Phys. **240,** 83–92 (1985).
39. B. E. A. Saleh and M. C. Teich, *Fundamentals of Photonics* (Wiley, 1991), pp. 351–352.
40. E. Akkermans, P. E. Wolf, and R. Maynard, "Coherent backscattering of light by disordered media: analysis of peak line shape," Phys. Rev. Lett. **56,** 1471–1474 (1986).